Predicting satellite-derived patterns of large-scale disturbances in forests of the Pacific Northwest Region in response to recent climatic variation

Richard H. Waring [a,*], Nicholas C. Coops [b], Steven W. Running [c]

[a] College of Forestry, Oregon State University, Corvallis, OR 97331, United States
[b] Department of Forest Resource Management, 2424 Main Mall. University of British Columbia, Vancouver, Canada V6T 1Z4
[c] College of Forestry & Conservation, University of Montana, Missoula, MT 59812, United States

ABSTRACT

Across the Pacific Northwest, the climate between 1950 and 1975 was exceptionally cool and wet compared with more recent conditions (1995–2005). We reasoned that the changes in climate could result in expanded outbreaks of insects, diseases, and fire. To test this premise, we first modeled monthly variation in photosynthesis and growth of the most widely distributed species, Douglas-fir (*Pseudotsuga menziesii*), using a process-based model (3-PG) for the two periods. To compare with remotely sensed variables, we converted modeled growth potential into maximum leaf area index (LAImax), which was predicted to range from 1 to 9 across the region. On most sites, varying soil moisture storage capacity (θcap) from 200 to 300 mm while holding soil fertility constant, made slight but insignificant difference in simulated LAImax patterns. Both values of θcap correlated well with LAI estimates acquired from NASA's MODIS satellites in June, 2005 ($r^2 = 0.7$). To evaluate where 15 coniferous tree species might be prone to wide-scale disturbance, we used climatically-driven decision-tree models, calibrated in the 1950–1975 period, to identify vulnerable areas in 1995–2005. We stratified predictions within 34 recognized ecoregions and compared these results with large-scale disturbances recorded on MODIS imagery acquired between 2005 and 2009. The correlation between the percent of species judged as vulnerable within each ecoregion and the percent of forested areas recorded as disturbed with a MODIS-derived Global Disturbance Index was linear and accounted for 65 to 73% of the observed variation, depending on whether or not disturbance by fire was excluded from the analysis. Based on climate projections through the rest of the rest of the 21st century, we expect continued high levels of disturbance in ecoregions located beyond the climatically buffering influence of the Pacific Ocean.

© 2011 Elsevier Inc. All rights reserved.

1. Introduction

Over the last three to four decades, forests throughout much of western North America have been subjected to disturbance at a scale well beyond that previously recorded over the last century (Raffa et al., 2008). Although some disturbances may be attributed to fire suppression policies, which have resulted in fuel accumulation and denser stands prone to insect attack (Coops et al., 2009a), climate change is more likely the cause, based on recent surveys and analyses of natural mortality caused by drought (Allen et al., 2010), bark beetles (Bentz et al., 2010; Raffa et al., 2008), needle blight (Woods et al., 2005), Swiss needle cast (Manter et al., 2005), a reduction in protective snow cover (Beier et al., 2008) and an increased frequency and intensity of wildfires (Westerling et al., 2006). Recent changes in climate are well documented in the Pacific Northwest Region of North America and the rates are predicted to accelerate (Mote et al., 2003; Mote & Salathe, 2010).

Many climatic-driven models have been developed to characterize and define the current recorded ranges of western tree species (e.g., Rehfeldt et al., 2006). These models, with the incorporation of more current climate data, have identified areas where drought and other factors appear to account for the extensive mortality observed on some native tree species (e.g. Rehfeldt et al., 2009). Although a variety of climatic indices of drought and changes in the length of the growing season are available (Jolly et al., 2005; Sutherst, 2003; Zhao & Running, 2010), few take into account species differences in temperature optima, rooting depth, and vulnerability to frost or drought.

Process-based models are available that accurately predict the growth of individual species (or genotypes) under changing environments, even well outside their native ranges (Landsberg et al., 2003). Such models, however, are largely designed for even-aged plantations where competition from other species is absence and climatic conditions are not lethally limiting. There are situations where environmental extremes do limit the distribution of tree species within their native ranges, but in the temperate climate of the Pacific

* Corresponding author. Tel.: +1 541 737 6087.
E-mail address: Richard.Waring@oregonstate.edu (R.H. Waring).

Northwest, such conditions are rare (Coops et al., 2009b; Waring & Franklin, 1979).

One advantage of process-based models is that they not only predict tree growth potential but the maximum display of leaf area (LAI_{max}), a variable that can be assessed remotely from space (Price & Bausch, 1995; White et al., 1997). Previous research in the Pacific NW documents that the LAI_{max} predicted for one species is similar to that recorded for broad mixtures of morphologically similar tree species (Spanner et al., 1994; White et al., 1997). Moreover, for evergreen conifers assessed in this paper, a linear relation exists between maximum growth potential and LAI_{max} (Waring, 1983; Waring et al., 2005).

To combine the strengths of process-based models with climatic indices keyed to individual species, Coops et al. (2009b) developed a hybrid approach, which progresses in a series of steps. First, a process-based model, which takes into account seasonal constraints on photosynthesis associated with humidity deficit of the air, suboptimal temperatures, the frequency of frost, and drought, predicts LAI_{max}. Secondly, decision-tree analysis are made (De'ath, 2002) to identify thresholds in the above-mentioned limiting factors that best predict the recorded presence and absence of different species on thousands of plots (Coops et al., 2009b; Coops et al., 2011). Finally, species-specific decision-tree models are rerun with different scenarios representing past, current, or future climatic conditions to map where a species remains well adapted or is judged vulnerable to disturbance and possible replacement by other species (Coops & Waring, 2011). In areas where a majority of native species become vulnerable, we would expect major disturbances.

In Coops et al. (2011), nine species were added to the six evaluated earlier (Coops et al. (2009b)), while extending the area analyzed to include parts of British Columbia and Alberta, Canada. The vulnerability of the 15 species was assessed and mapped in reference to changes in climatic conditions between two periods: 1950–1975 and 1976–2006, and the results discussed in reference to four large subregions (Coops & Waring, 2011). In this paper we narrow the comparison to the period between 1995 and 2005 in recognition that MODIS-derived products commensurable with our modeling resolution (1 km) are available only since the launch of NASA's Terra and Aqua satellites in 2000 and 2002, respectively. We also analyze the results in finer detail among 34 designated EPA level III ecoregions[1] (Fig. 1).

Disturbances, both large and small, have been a focus of satellite remote sensing since the launch of the first Landsat series in 1974 (Cohen & Goward, 2004). In forested areas, major disturbances caused by fire, logging, wind throw, and shifts in land use can be readily identified (Foody et al., 1996; Rignot et al., 1997), as well as more subtle disturbances associated with tree thinning, insect outbreaks, and changes in forest composition (see reviews by Gong & Xu, 2003; Coppin et al., 2004; Franklin, 2010).

A disturbance causes a relative reduction in canopy greenness and a relative increase in the surface integrated temperature (Goward et al., 1985). Mildrexler et al. (2007, 2009) capitalized on the relationship between canopy greenness and thermal signal to create a Global Disturbance Index (GDI) at 1 km² resolution using NASA's moderate resolution imaging spectroradiometer (MODIS). The GDI will be described in more detail in Section 2.6.

We reference remotely sensed imagery in two ways: first, to make a general comparison with modeled estimates of LAI_{max}, and secondly, with the derivation of GDI, to document the extent that forested areas within 34 defined ecoregions were disturbed between 2005 and 2009. In the latter case, the disturbed areas were compared with those predicted to be occupied by species in the cool, wet period (1950–1975) and judged vulnerable in response to changes in climatic conditions for the period 1995–2005.

---

[1] http://www.epa.gov/wed/pages/ecoregions/na_eco.htm#LevelIII.

2. Data and methods

2.1. Major vegetation zones within the study area

The Pacific Northwest Region, which extends from northern California to British Columbia and inland to western Montana, includes portions of four broad subregions (http://www.epa.gov/wed/pages/ecoregions/na_eco.htm#LevelI). The most productive component is included in the Marine West Coast Forest zone, which extends from Alaska in a progressively narrowing band to San Francisco. Western hemlock (*Tsuga heterophylla*) and Sitka spruce (*Picea sitchensis*) are present throughout most of this fog-belt defined zone, with Douglas-fir (*Pseudotsuga menziesii*), coast redwood (*Sequoia sempervirens*), Alaska yellow cedar (*Chamaecyparis nootkatensis*), western red cedar (*Thuja plicata*) and grand fir (*Abies grandis*) well represented in some areas. The Northwest Forested Mountains is the second most productive subregion in the study area. Douglas-fir and western hemlock are frequently abundant in mixtures with Pacific silver fir (*Abies amabilis*), noble fir (*Abies procera*) and western larch (*Larix occidentalis*). At higher elevations and latitudes, lodgepole pine (*Pinus contorta*), whitebark pine (*Pinus albicaulis*), mountain hemlock (*Tsuga mertensiana*), subalpine fir (*Abies lasiocarpa*), and Engelmann spruce (*Picea engelmannii*), are characteristic species.

On drier sites, ponderosa pine (*Pinus ponderosa*) and incense cedar (*Calocedrus decurrens*) are usually present. Ponderosa pine extends its range southward into the fringe of the North American Desert, with further reductions in productivity. In Oregon and northern California, in the rain shadow of the Cascade Mountains, open pine forests grade into western juniper (*Juniperus occidentalis*) woodlands and finally to sagebrush steppe (Franklin & Dyrness, 1973; Runyon et al., 1994). Beyond the influence of summer intrusions of maritime air masses, a small component of the Mediterranean California zone is included within the PNW region where oaks (*Quercus*), pines and Douglas-fir occur in a transition to grasslands and chaparral (Waring & Major, 1964).

2.2. Historical and projected variation in regional climate

Historically, climatic variation in the Pacific Northwest has been linked with shifts in the warm and cool phases of the Pacific Decadal Oscillations (PDO) in combination with the El Niño Southern Oscillation (ENSO). When both the PDO and ENSO enter a positive phase, winters are much drier and warmer than normal, and summers somewhat more drought-prone. When negative phases of the two oscillations correspond, winters are much cooler and wetter than normal, resulting in higher than average snowpack, more runoff, and a reduced chance of summer drought and late season fires (Mote et al., 2003).

The PDO was in an extended cool phase from about 1890 to 1925 and from 1945 through 1976. From 1925 to 1946 and from 1977 to 1998, a warm phase of the PDO dominated. Since 1650, there has been 11 major phase shifts in the PDO, each averaging 23 years (Gedalof & Smith, 2001). Recently, the PDO has shifted back and forth from one phase to another, more typical of patterns in the 19th century (Mantua, 2001). Trouet and Taylor (2009) estimated the combined effects of PDO and ENSO on the Pacific North American circulation pattern to be more variable during the 1960s than the PDO record would indicate, but noted that that the cool (negative) phase of the PNA extended unbroken from the early 1950s back to 1941. Over the past half century, the Pacific Northwest has experienced significant climate variability, especially at the higher latitudes, creating conditions that may have altered the ecological fitness of native species in much of their currently recorded ranges.

Most climate models predict that the Pacific Northwest region as a whole will become progressively warmer by 2–5° by 2080, with perhaps somewhat more precipitation in the winter and spring, and less during the summer (Mote et al., 2003; Mote & Salathe, 2010). These trends accentuate those observed over the past century. The
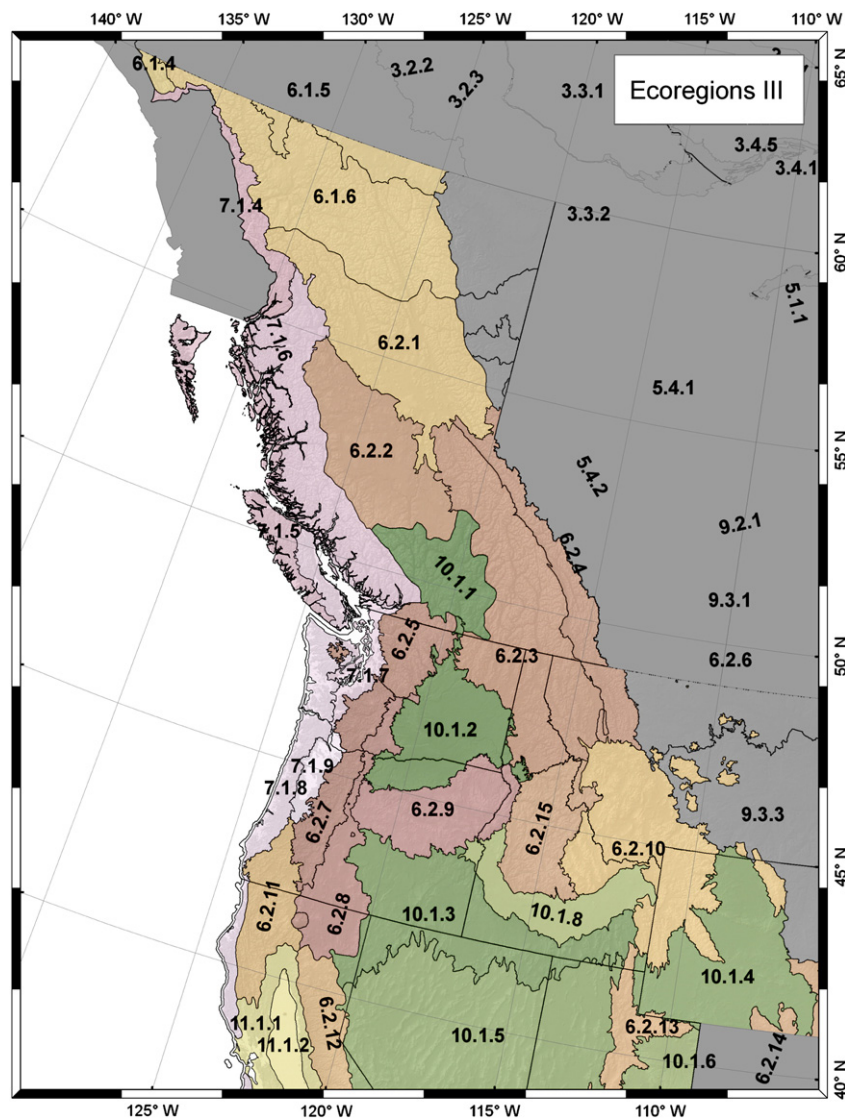
Fig. 1. Defined boundaries of the Environmental Protection Agency's 34 level III ecoregions.

largest changes are predicted to occur to the north, particularly in inland British Columbia and Alberta. In those areas, the frost-free period is expected to increase by at least a month and periods of extremely warm summer days are likely to become more common, with the high emission scenario leading to mean annual temperatures increases by 2080s of 3–5 °C (Spittlehouse, 2008).

2.3. Climatic data

Long-term weather observations for stations throughout the region were interpolated spatially using Climate-WNA (http://www.genetics.forestry.ubc.ca/cfcg/ClimateWNA/ClimateWNA.html), which includes a bilinear interpolation of the PRISM (Parameter-elevation Regressions on Independent Slopes Model) records, along with adjustments in temperature for mountainous terrain (Wang et al., 2006). A 90 m-Digital Elevation Model (DEM), obtained from the Shuttle Radar Topography Mission (SRTM), was expanded to 1 km to provide the required elevation data at the same resolution as the climatic data.

Mean monthly daytime vapor pressure deficits (VPD) were estimated by assuming that the water vapor concentrations present throughout the day would be equivalent to that held at the mean minimum temperature (Kimball et al., 1997). The maximum VPD was calculated each month as the difference between the saturated vapor pressure at the mean maximum and minimum temperatures. Mean daytime VPD was calculated at two thirds of the maximum value (Waring, 2000). The number of days per month with subfreezing temperatures (≤ 2 °C) was estimated from empirical equations with mean minimum temperature (Coops et al., 1998). In modeling, we did not attempt to account for extremes in temperature that might kill native species because representatives of most conifers present in the region have survived for at least the last 50 years and in many cases a half a millennium or more (Waring & Franklin, 1979).

Monthly estimates of total incoming short-wave radiation were calculated using a modeling approach detailed by Coops et al. (2000) where the potential radiation reaching any spot is first calculated and then reduced, based on the clarity (transmissivity) of the atmosphere. Changes in the atmospheric transmissivity are mirrored in temperature extremes (Bristow & Campbell, 1984). With a digital elevation model, we adjusted for differences in slope, aspect, and elevation as well as for variations in the fraction of diffuse and direct solar beam radiation (Hungerford et al., 1989). The modeling approach, when compared with direct measurements, predicted both the direct and diffuse components of mean monthly incoming radiation with 93–99%

accuracy on flat surfaces, and on sloping terrain accounted for >87% of the observed variation with a mean error <2 MJ m^{-2} day^{-1} (Coops et al., 2000).

2.4. Process-based growth model

There are a wide variety of physiologically-based process models available but only a few have been designed to scale projections of photosynthesis, structural growth, and mortality across landscapes (see reviews by Mäkelä et al., 2000; Nightingale et al., 2004). Among the most widely used is the 3-PG model (Physiological Principles Predicting Growth) developed by Landsberg and Waring (1997). The 3-PG model include the following simplifications: a) that monthly mean climatic data are adequate to capture major trends, b) that for each month, knowledge of the most limiting variable constraining photosynthesis is sufficient, c) that autotrophic respiration (R_a) and net primary production (P_{net}) are approximately equal fractions of gross photosynthesis (P_g), d) that maximum canopy conductance approaches a constant as LAI exceeds 3.0, and e) that the proportion of photosynthate allocated to roots increases with drought and decreases with nutrient availability.

Previous to this study, we parameterized the 3-PG model for Douglas-fir using data from both conventional forestry yield tables and other sources (Coops et al., 2011; Waring & McDowell, 2002). In this paper, we use those published parameter values with a few exceptions (Table 1). To limit the analysis to climatic effects, we initially set the available water holding capacity, θ_{cap}, at 200 mm for a sandy loam soil, a value that assures that if drought occurs, it will be recognized (Coops et al., 2001; Nightingale et al., 2007). Comparisons performed at 40 widely distributed, diverse sites support the appropriateness of using a common value for θ_{cap} of 200 mm (Coops et al., 2001; Coops & Waring, 2001). In this study, we make a region-wide comparison of changes in simulated LAI$_{max}$ with θ_{cap} set not only at 200 but also 300 mm.

Although generalized regional soils maps are available from the U.S. Conservation Service State Soil Geographic Data Base (STATSGO), their accuracy, even at a spatial resolution of 1 km, has proven inadequate for most forest ecosystem analyses (Coops & Waring, 2001; Lathrop et al., 1995; Swenson et al., 2005; Zheng et al., 1996). Because of the inaccuracies of STATGSO products, as well as the lack of a systematic comparison in western Canada, we assign the same default values of θ_{cap} and soil fertility to all sites in our climate-change assessment.

Specifically, a soil fertility rank of 50% of maximum was chosen as a default value, which results in an even partitioning of growth above- and below ground (Table 1). Because soil fertility also affects the quantum efficiency (α), representing the linear rate that absorbed light is converted into photosynthetic products, we set α at a fixed value of 0.045 mol C mol photon^{-1}, equivalent to 2.48 g C MJ^{-1} absorbed PAR, about mid-way between reported minimum and maximum values in the literature (Landsberg et al., 2003). We recognize that variation in soil fertility across the region affect productivity, and thus LAI$_{max}$ (Coops & Waring, 2001; Huston & Wolverton, 2009; Swenson et al., 2005). Alternative procedures for assessment of soil fertility will be discussed in Section 4.2.

To account for seasonal adjustments in temperature optima (Hember et al., 2010) and the genetic variation among populations of Douglas-fir, we broadened the range that photosynthesis could remain above 50% of maximum to lie between 0 °C and 35 °C by setting minimum, optimum, and maximum temperatures at −7 °C, 18 °C, and 40 °C, respectively. The photosynthetic response at temperatures <−2 °C was truncated to zero, because below that threshold stomata are closed (Hadley, 2000; Running et al., 1975).

Following procedures outlined in Coops et al. (2009b), we assessed the implications of the seasonal limitations of water availability, deviations from the optimum temperature (18 °C), frost frequency (days<−2 °C), and atmospheric humidity deficits (VPD) on photosynthesis and growth. The link to photosynthesis is important because the potential varies seasonally. The upper limits are set by the amount of light absorbed by green leaves (LAI). Thus a day of subfreezing temperatures in the winter, when the day length is short in the Northern Hemisphere, has much less effect on photosynthesis than in May when the day length is much longer and incident radiation higher. Predictions of LAI$_{max}$ were extracted along with monthly environmental limitations to photosynthesis after establishing a forest and growing it to an age of 50 years in each, sequentially processed simulation. Modeled monthly LAI sets limits on transpiration and interception of solar radiation, the latter which changes significantly with latitude as well as slope, aspect, and season.

2.5. Climate-driven decision-tree models

To develop species-specific decision-tree models, a suite of rules were created, automatically, to identify physiological thresholds that differ among species, and therefore can serve to predict a species' presence or absence on survey plots. On the basis of these rules, created from climatic conditions typical of the defined baseline period, 1950–1975, Coops et al. (2011) predicted where 15 species of western conifers should be distributed on 22,771 sites with reasonable accuracy (average agreement of 82%, with a range between 70% and 95% for both presence and absence). As one might expect, a subalpine species tolerates more frost in the spring, occupies cooler sites in the summer, and experiences less evaporative demand and drought than do more temperate species such as Douglas-fir and western hemlock. The climatic conditions to which subalpine species are well adapted also restrict their inherent growth rates. Similarly, where western juniper, incense cedar, and ponderosa pine occur on drought-prone sites, changes in precipitation patterns may alter the competitive status of one species with another, leading to a shift in forest composition.

Once species-specific decision-tree models were developed for the calibration period, we ran them with climatic data from 1995 to 2005 to judge whether conditions had changed sufficiently so that some species would no longer be predicted to be as well adapted as previously.

Table 1
3PG parameters used in the study.

| Variable	Functions and parameter values	Source
Light conversion efficiency of photosynthesis	2.48 g C MJ^{-1} absorbed PAR	Waring and McDowell (2002)
Temperature limits on light conversion	$T_{min} = -7$ °C, $T_{opt} = 20$ C, $T_{max} = 40$ °C	T_{min} this study Waring and McDowell (2002)
% light absorbed by canopy	1 − (2.718 exp (−0.5 LAI) 100	Landsberg and Waring (1997)
Soil fertility ranking	50% of maximum	This study
Soil water storage capacity	200 and 300 mm	This study
Max leaf stomatal conductance	0.006 m s^{-1}	Waring and McDowell (2002)
Max canopy conductance	0.018 m s^{-1}	Waring and McDowell (2002)
Stomata response (gc) to VPD (mb)	gc = gcmax^ (−0.5 VPD)	Landsberg and Waring (1997)
Specific leaf area	6.0 m^2 kg^{-1}	Waring and McDowell (2002)
Leaf turnover each month	2.1%	Waring and McDowell (2002)
Allometric Eq., stem mass (kg)	= 0.0843 (dia., cm) ^2.436	Waring and McDowell (2002)
Allometric Eq., foliage prod. (kg)	= 0.1484 (dia.,cm) ^2.533	Waring and McDowell (2002)
Wood density	450 kg m^{-3}	Waring and McDowell (2002)
Age approaching max height	200 years	Waring and McDowell (2002)
Fraction of growth to roots	50%	This study
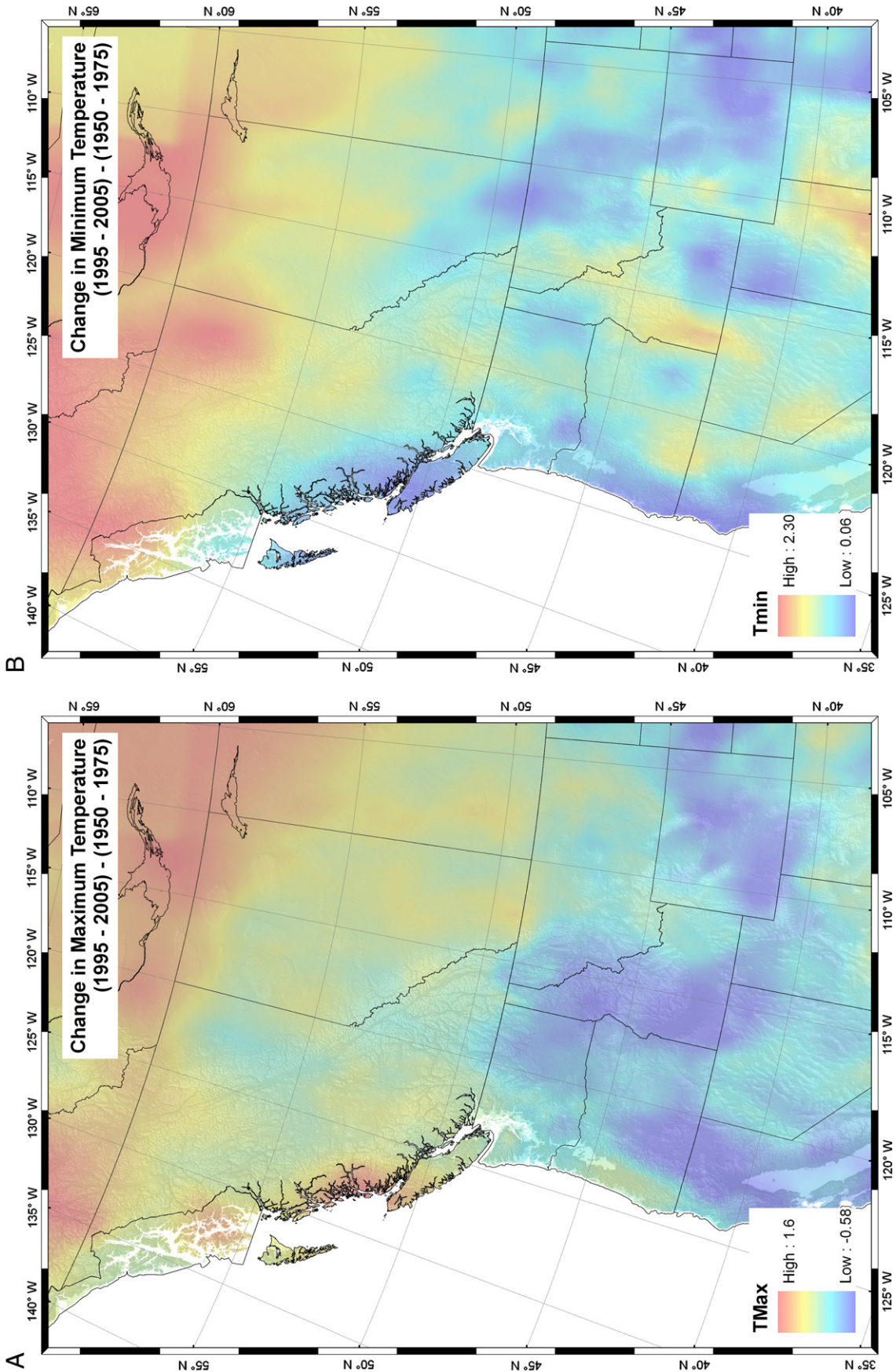
Fig. 2. Regional changes in climatic conditions between two periods (1995–2005)–(1950–1975). (A) mean annual maximum temperature, (B) mean annual minimum temperature, and (C) mean annual precipitation.
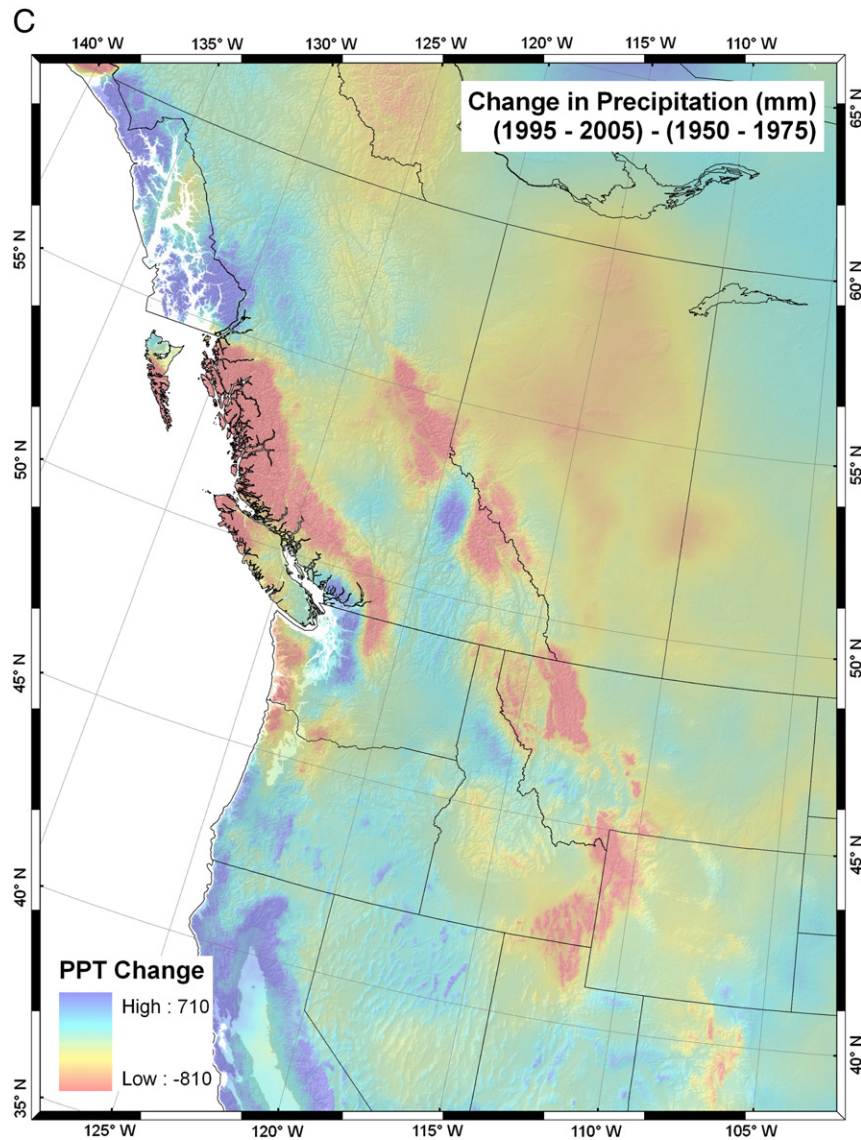
Fig. 2 (*continued*).

The forested areas in which such species were judged vulnerable to a changing climate were then compared in each of the 34 ecoregions. The mean vulnerability of those species originally predicted to be present in each ecoregion was then calculated, and the two most vulnerable species were identified if they occupied >5% of the delineated forested area.

2.6. Global Disturbance Index

The GDI values at a spatial resolution of 1 km for the period 2005–2009 were processed by the Numerical Terradynamic Simulation Group (NTSG) at the University of Montana. The disturbance index was created using an algorithm detailed in Mildrexler et al. (2009). In brief, the algorithm requires an annual maximum land surface temperature (LST) and maximum enhanced vegetation index (EVI) from a sequence of annual MODIS observations. The ratios of these annual values (2005–2009) were then compared to mean ratio values derived from 2000 to 2005 data. Annual ratios that exceeded ±1 standard deviation from the 2000 to 2005 values were assumed to represent some kind of disturbance. GDI values were filtered to remove false detection associated with uncertainties in the MODIS

EVI and LST products introduced by background noise, which becomes apparent when pixels representing disturbance become spatially scattered.

Only cells recognized as woodlands or forests, based on the MODIS land-cover classification, were included in the analysis (following procedures in Mildrexler et al., 2009). To distinguish if disturbances detected with the GDI products were caused by fire, we utilized MODIS hotspot data from the Fire Information for Resource Management System (FIRMS). The accuracy of the MODIS hotspot algorithm has been independently validated with data acquired from NASA's Advance Spaceborne Thermal Emission and Reflection Radiometer, ASTER (Justice et al., 2002). We downloaded hotspot data acquired from 2006 to 2009 and gridded it to 1 km spatial resolution to match the GDI data.

The areas of woody vegetation within each of 34 level III ecoregions in the Pacific Northwest region (U.S. Environmental Protection Agency (EPA)) were computed to serve as a basis for calculating the percentage disturbed over the period from 2005–2009. With regression analysis we compared the number of pixels flagged as disturbed by the MODIS algorithm with the proportion of the species in each of the ecoregions deemed vulnerable.
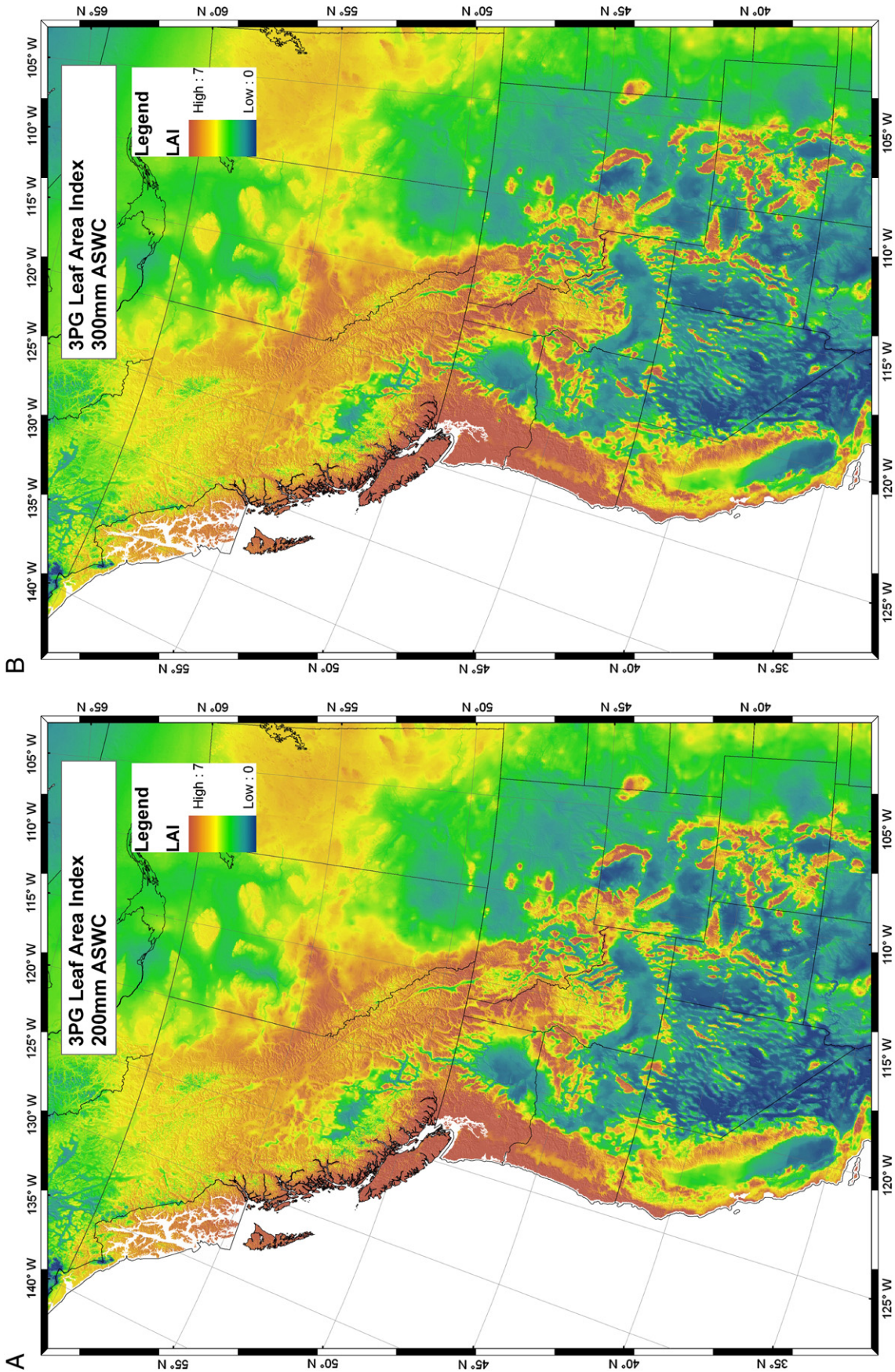
Fig. 3. Simulated maximum leaf area index (LAI$_{max}$) with available soil water storage capacity set at (A) 200 mm and (B) 300 mm, compared with (C) MODIS-derived estimates of LAI$_{max}$ for June, 2005. Simulated values of LAI > 7.0 were truncated to 7.0 to match maximum values provided from MODIS imagery.
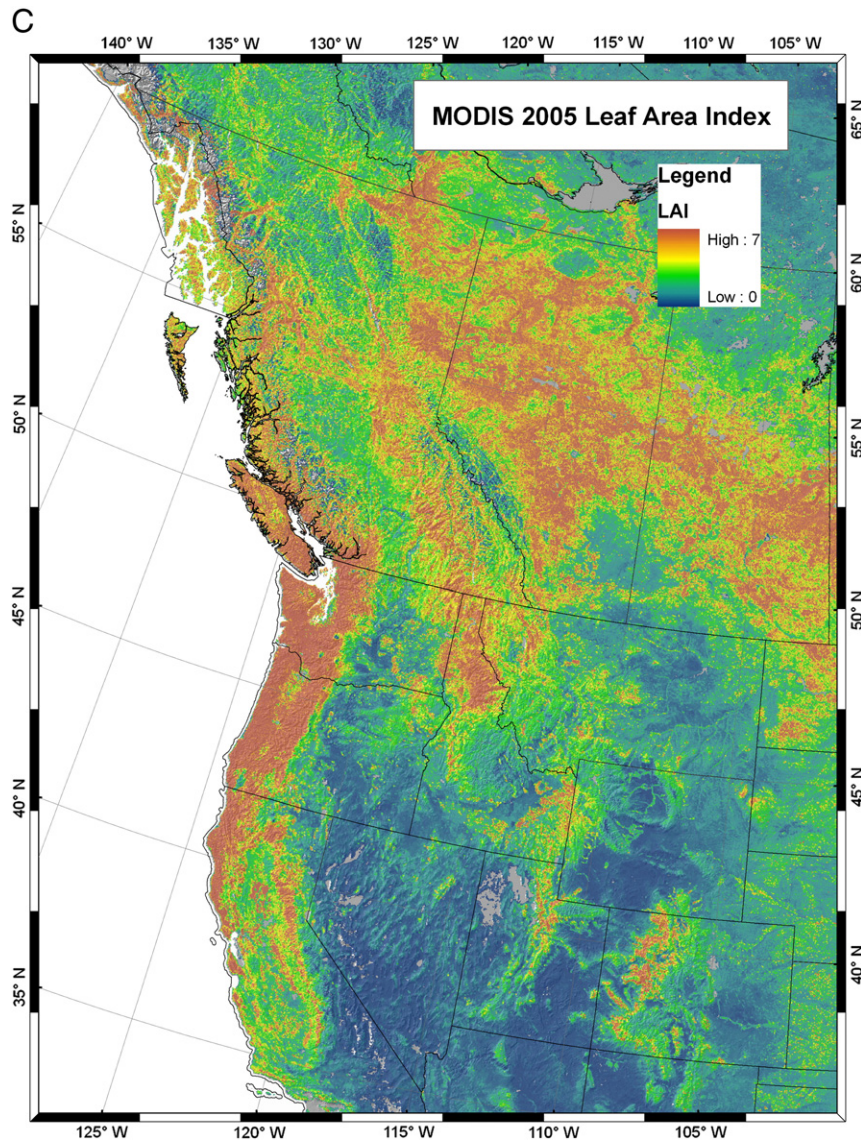
C

Fig. 3 (*continued*).

3. Results

3.1. General trends in climate

Since the predominantly cool, wet period (1950–1975), there has been a notable warming trend in western Canada, and a reduction in annual precipitation of >800 mm in some places in the Coast Range of British Columbia and Washington State as well as through the Rocky Mountains (Fig. 2). These trends are consistent for all seasons (data not shown) and have particular significance in the spring and fall. A reduction in winter precipitation results in less accumulation of snow. Combined with warmer temperatures in the spring, the start of the growing season is advanced. Warmer temperatures during the summer, combined with less precipitation in the fall, lead to drought and an increased probability of fire in some places (Mote et al., 2003).

3.2. Comparison of LAI_max predicted with 3-PG model and that derived from MODIS imagery

Varying the θ_{cap} value between 200 and 300 mm resulted on average, in only a 0.2 increase in simulated LAI_max across ecoregions

(Fig. 3a and b, Table 2). In contrast, LAI_{max} values derived from MODIS imagery (Fig. 3b) averaged nearly 2.0 units lower than values predicted with 3-PG simulations, significant at p<0.05 (Table 2). 3-PG predictions of LAI_{max} were generally well correlated with MODIS-derived values ($r^2 = 0.7$), although significantly higher (p<0.05).

3.3. Mapped areas of species vulnerability

Fig. 4(a) maps the proportion of conifer species in each of 34 ecoregions predicted to reside under less favorable competitive conditions in the period from 1995 to 2005 than during the cooler and wetter years between 1950 and 1975. A more detailed analysis is provided in Table 3. The Pacific Northwest Region, according to this analysis, has seen a significant decrease in the competitiveness of over 50% of the evergreen species in a half dozen ecoregions, with the highest concentration towards the northern and southern limits of our analysis (Table 3: EPA codes: 6.1.5, 10.1.3, 10.1.4., 10.1.5., 10.21; see Fig. 1). In contrast, species distributed in ecoregions nearer the Pacific Coast were judged to have changed little in their vulnerability to disturbance from the baseline period (Table 3: Ecoregions: 7.14, 7.1.5, 7.1.6, 7.17, 7.1.8).

Table 2
Comparison of predicted LAI$_{max}$ from 3PG using 200 and 300 mm soil water storage and observed MODIS LAI.

LEVEL 3		3PG LAI 200 mm	STD	3PG LAI 300 mm	STD	MODIS LAI	STD
10.1.1	Thompson-Okanogan Plateau	5.81	1.26	6.04	1.26	3.29	1.26
10.1.2	Columbia Plateau	3.57	1.48	3.69	1.61	2.10	1.55
10.1.3	Northern Basin and Range	3.42	1.45	3.53	1.55	1.11	0.89
10.1.4	Wyoming Basin	2.75	1.20	2.85	1.25	0.81	0.80
10.1.5	Central Basin and Range	2.28	1.05	2.34	1.14	0.74	0.63
10.1.6	Colorado Plateaus	2.83	1.35	2.87	1.39	0.79	0.85
10.1.8	Snake River Plain	2.68	1.13	2.75	1.25	2.00	1.55
10.2.1	Mojave Basin and Range	1.82	0.89	1.71	0.90	0.53	0.35
11.1.1	California Coastal Sage, Chaparral, and Oak Woodlands	4.97	1.36	5.26	1.57	3.20	1.42
11.1.2	Central California Valley	3.17	1.12	3.24	1.41	3.15	1.59
11.1.3	Southern and Baja California Pine-Oak Mountains	5.57	1.19	5.76	1.29	2.26	1.25
5.4.2	Clear Hills and Western Alberta Upland	6.54	0.60	6.71	0.52	4.50	1.19
6.1.5	Watson Highlands	4.60	0.91	4.98	0.94	2.66	1.13
6.1.6	Yukon-Stikine Highlands/Boreal Mountains and Plateaus	5.45	0.69	5.75	0.69	2.52	1.38
6.2.1	Skeena-Omineca-Central Canadian Rocky Mountains	6.51	0.52	6.76	0.42	3.83	1.33
6.2.10	Middle Rockies	5.49	1.48	5.72	1.52	2.24	1.17
6.2.11	Klamath Mountains	6.05	0.89	6.57	0.63	4.98	1.44
6.2.12	Sierra Nevada	5.78	1.18	6.42	0.96	3.24	1.77
6.2.13	Wasatch and Uinta Mountains	5.17	1.69	5.43	1.73	2.41	1.48
6.2.14	Southern Rockies	5.17	1.48	5.41	1.55	2.29	1.46
6.2.15	Idaho Batholith	5.99	0.91	6.48	0.84	2.66	1.35
6.2.2	Chilcotin Ranges and Fraser Plateau	5.18	1.21	5.51	1.28	2.95	1.23
6.2.3	Columbia Mountains/Northern Rockies	6.46	0.80	6.66	0.73	4.16	1.42
6.2.4	Canadian Rockies	6.65	0.62	6.78	0.54	3.15	1.48
6.2.5	North Cascades	6.67	0.78	6.81	0.64	4.38	1.66
6.2.7	Cascades	6.90	0.33	6.98	0.18	5.36	1.32
6.2.8	Eastern Cascades Slopes and Foothills	5.16	1.22	5.75	1.28	2.50	1.55
6.2.9	Blue Mountains	5.11	1.67	5.31	1.73	1.99	1.14
7.1.4	Pacific Coastal Mountains	5.41	1.50	5.64	1.53	3.62	2.16
7.1.5	Coastal Western Hemlock-Sitka Spruce Forests	6.89	0.33	6.93	0.25	4.35	1.29
7.1.6	Pacific and Nass Ranges	6.47	0.80	6.62	0.71	4.23	1.66
7.1.7	Strait of Georgia/Puget Lowland	7.00	0.02	7.00	0.01	5.47	1.22
7.1.8	Coast Range	6.94	0.23	6.99	0.06	5.90	1.06
7.1.9	Willamette Valley	6.91	0.16	7.00	0.00	5.35	1.26

Subalpine species appeared among the most vulnerable to recent climatic variation, listed as >50% vulnerable in 2/3th of 34 ecoregions (Table 3), with lodgepole pine leading the field in 10 ecoregions. Sitka spruce, a species with a restricted range near the Pacific Coast, was notably absent for the assessment of highly vulnerable species, but this in part is an expression of its restricted limits within an ecoregion (Coops & Waring, 2011).

3.4. Mapped areas of recent disturbance

Disturbances are mapped in Fig. 4b based on GDI values acquired from 2005 to 2009 in referenced to baseline conditions recorded between 2000 and 2005. The largest disturbances over the four years of observations

were recorded in British Columbia and California. In general, disturbance by fire increases toward the south.

3.5. Modeled versus remotely sensed disturbance patterns

Fig. 5 presents a comparison between the proportion of species in each ecoregion designated as highly vulnerable (Fig. 4a) and the areas recognized as recently disturbed from the GDI, (Fig. 4b). The comparison with areas that do not include disturbance by fire (Fig. 5a) has somewhat higher correlations ($r^2 = 0.73$ versus 0.64) with areas predicted to be vulnerable than when fire is included with other disturbances (Fig. 5b).

4. Discussion

4.1. Comparing LAI$_{max}$ predictions

Although the regressions between 3-PG estimates of LAI$_{max}$ and those derived from MODIS imagery were highly correlated ($r^2 = 0.7$), the former averaged nearly two units higher. The difference would be even larger had we not reduced 3-PG estimates above 7.0 to match the maximum values reported for MODIS. We do not believe that these discrepancies can be attributed to large, unrecognized disturbances because ground vegetation normally reestablishes quickly on forested sites throughout the region (Law et al., 2004).

Based on previous modeling efforts to estimate productivity (Swenson et al., 2005), and differences reported in the concentration of exchangeable bases across the region (Huston & Wolverton, 2009), we expect that some of the deviations between predicted and observed values of LAI$_{max}$ reflect variation in soil fertility, which we ignored by setting default value of 0.5 of maximum (Table 1). Potentially, the range in soil fertility across the region is sufficient to permit photosynthetic efficiency and the partitioning of growth above- and belowground to vary by more than two-fold (Landsberg et al., 2003).

4.2. Alternative to STATSGO mapping of soil fertility

Most soil maps, regardless of the scale, are unable to take into account shifts in soil fertility associated with disturbance and recovery. Stand-replacing fires generally reduce nitrogen availability while increasing that of potassium, calcium, and magnesium. Normally, disturbed sites are rapidly colonized by nitrogen-fixing genera (e.g., Alnus, Ceanothus, Lupinus) that significantly increase soil fertility (Waring & Running, 2007). Following an idea proposed by Landsberg & Waring (2004), we might derive better maps of soil fertility by adjusting estimates of that variable with the 3-PG model to achieve the best fit between predicted and MODIS-derived estimates of LAI$_{max}$.

4.3. Predicting disturbances, currently and in the future

By separating fire from other types of disturbance, we confirmed the general expectation that fire becomes more important in the region at more southern latitudes, while insect and disease outbreaks are likely, at least initially, to be more prevalent moving northward. The point in common is that disturbances across a wide assortment of ecoregions show a differential proportion of forested areas recently disturbed that is correlated with the proportion of tree species deemed less competitive in those locations than they were previously. Note that the area predicted as vulnerable to disturbance is much larger than that recorded between 2005 and 2009 (compare Fig. 4a with 4b). In part, this difference can be attributed to recovery of LAI$_{max}$ following extensive outbreaks of insects and diseases as documented from aerial surveys over much a longer period (Raffa et al., 2008; http://svinetfc8.fs.fed.us/aerialsurvey/).

At higher elevations, subalpine tree species are known to be well adapted to frost and heavy snow loads. With a general reduction in snow cover and less spring frost, subalpine species commence their
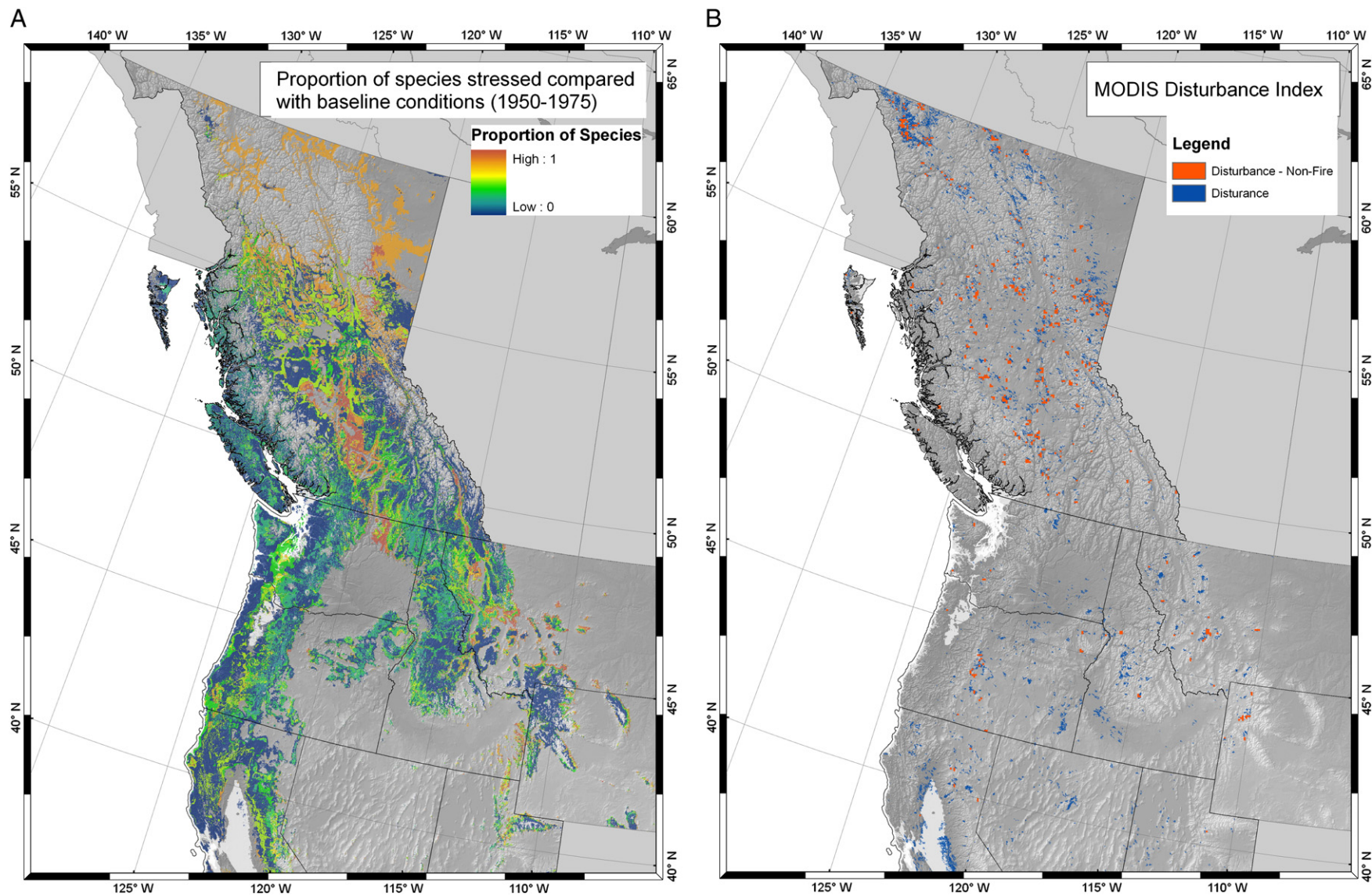
Fig. 4. (A) Map presenting the proportion of fifteen coniferous species predicted as no longer well adapted in the years 1995–2005 compared with baseline conditions (1950–1975). (B) The distribution of cells recognized as disturbed between 2005–2009 by any cause (blue) and those with fire excluded (red) based on analysis with the MODIS Global Disturbance Index in combination with the MODIS hotspots analysis for the period 2005–2009.

Table 3
Decision-tree modeling of species' mean % vulnerability in 34 ecoregions. The 1st and 2nd most vulnerable species in each ecoregion are listed if they were modeled to occur in >5% of the forested area and were judged >50% vulnerable.

Ecoregion	EPA code	1st species	2nd species	Mean % Vulnerability
Clear Hills and Western Alberta Upland	5.4.2	ENG	DF	36
Watson Highlands	6.1.5	ENG	WP	68
Yukon-Stikine Highlands/Boreal Mountains and Plateaus	6.1.6	ENG	WP	40
Skeena-Omineca-Central Canadian Rocky Mountains	6.2.1	WP	ENG	34
Chilcotin Ranges and Fraser Plateau	6.2.2	WL	–	23
Columbia Mountains/Northern Rockies	6.2.3	LPP	–	17
Canadian Rockies	6.2.4	–	–	20
North Cascades	6.2.5	YC	–	15
Cascades	6.2.7	LPP	–	13
Eastern Cascades Slopes and Foothills	6.2.8	LPP	MH	26
Blue Mountains	6.2.9	LPP	WH	27
Middle Rockies	6.2.10	WL	MH	38
Klamath Mountains	6.2.11	WH	–	26
Sierra Nevada	6.2.12	WH	MH	46
Wasatch and Uinta Mountains	6.2.13	MH	WRC	47
Southern Rockies	6.2.14	SAF	–	35
Idaho Batholith	6.2.15	WH	–	20
Pacific Coastal Mountains	7.1.4	ENG	WP	26
Coastal Western Hemlock-Sitka Spruce Forests	7.1.5	WP	–	19
Pacific and Nass Ranges	7.1.6	ENG	LPP	17
Strait of Georgia/Puget Lowland	7.1.7	PP	–	29
Coast Range	7.1.8	YC	PP	21
Willamette Valley	7.1.9	PP	–	32
Thompson-Okanogan Plateau	10.1.1	LPP	–	24
Columbia Plateau	10.1.2	LPP	WH	49
Northern Basin and Range	10.1.3	WRC	PSF	52
Wyoming Basin	10.1.4	PSF	GF	69
Central Basin and Range	10.1.5	MH	LPP	60
Colorado Plateaus	10.1.6	LPP	WL	49
Snake River Plain	10.1.8	LPP	–	34
Mojave Basin and Range	10.2.1	PP	DF	80
California Coastal Sage, Chaparral, and Oak Woodlands	11.1.1	WP	MH	58
Central California Valley	11.1.2	DF	–	52
Southern and Baja California Pine-Oak Mountains	11.1.3	PP	DF	59

DF = Douglas-fir, ENG = Engelmann spruce, GF = grand fir, LPP = lodgepole pine, MH = mountain hemlock, PP = ponderosa pine, PSF = Pacific silver fir, SAF = subalpine fir, SS = Sitka spruce, WH = western hemlock, WL = western larch, WP = white pine, WRC = western red cedar, YC = yellow cedar.

growing season earlier (Running, 1980, 1984). An earlier growing season has been tentatively documented with passive remote sensing (White et al., 2009). But with a reduction in environmental constraints on photosynthesis, conditions also have become more favorable for outbreaks of diseases and insects (Bentz et al., 2010; Woods et al., 2005). At the same time, more temperate species such as Douglas-fir (*P. menziesii*), grand fir (*A. grandis*), and western hemlock (*T. heterophylla*) are favored to invade and eventually replace the current dominants (Coops & Waring, 2011).

The warming trends that encourage growth at higher elevations and latitudes have increased drought at the other extremes (but see Crimmins et al., 2011). This warming trend has been attributed to causing a general increase in the frequency of fire across the western states (Westerling et al., 2006) and replacement of more drought-prone species with those more resistant (Allen & Breshears, 1998; Thorne et al., 2008).

Because climatic warming trends are projected to continue under a range of greenhouse gas emission scenarios (IPCC, 2007), new equilibrium conditions may not soon occur (Jackson et al., 2009; Thuiller et al., 2008). We would expect additional disturbance in those ecoregions with substantial subalpine zones and well as those

where drought is becoming more frequent and intense. The exception is those ecoregions within the maritime influence of the Pacific Ocean, which seem well buffered against climatic alterations that would favor replacement of the current mix of native tree species (Coops & Waring, 2011).

4.4. Alternative models and measurements

There are many models that might be substituted for the ones used in this paper. Rather than calculate a soil water balance, one could, for example, substitute a simple drought index calculated from climatic variables without regard to variation in LAI (e.g., Churkina & Running, 1998). Alternatively, LAI could, if satellite coverage were available, be estimated from that source (Churkina & Running, 1998; Coops et al., 1998; Nemani et al., 1996; Turner et al., 2006).

Similarly, in estimating species' distributions, there are many approaches available that utilize temperature and precipitation patterns and a host of climatic and physiographic indices to predict species' distributions without requiring estimates of solar radiation, vapor pressure deficits, LAI or a soil water balance (Iverson & Prasad, 1998; Rehfeld et al., 2006). Because of the large number of variables and more sophisticated sampling and analytic schemes employed in these approaches, however, it is difficult to explain functionally how they account for variation in the vulnerability of one species compared with another (Coops et al., 2011). Nevertheless, there is genuine value to having predictions derived from a wide range of models based on different assumptions, particularly if those predictions can be compared with field measurements and satellite-derived information. The approach used in this study has advantages in that it identifies variables that can be measured directly in the field: plant water stress, frost damage, soil water deficits, photosynthesis, stomatal conductance and growth, as well as changes in forest composition.

4.5. Role of remote sensing

By using models that predict LAI_{max}, define the growing season, and indicate the probability of fire or other types of disturbances, the approach presented in this paper offers the opportunity for remote sensing to serve as a truly independent validation (or falsification) test. If agreement between model predictions and observations are consistent, the possibility of forecasting the future implications of climatic variation on species diversity and vulnerability are measurably enhanced.

Further refinements in the remote sensing of LAI_{max} are clearly desirable. For example, photosynthetic capacity, a function of soil fertility, can be more accurately sampled with higher spectral resolution than available with instruments borne on current satellites (Whitehead et al., 2005). Radar and Lidar together promise significant improvements in measuring LAI and in separating overstory from understory components (Lefsky et al., 2002; Treuhaft et al., 2009). Similarly, improvements in defining the start and end of the growing season are in the offering using radar where subfreezing conditions occur (Kimball et al., 2004). Finally, Landsat imagery, with 30×30 m resolution, and a time series starting in 1974 offers the opportunity to define the kind of disturbance and the frequency beyond that obtained with MODIS (Huang et al., 2010).

5. Conclusion

The approach presented in this paper builds on two previously published models: one, 3-PG, which incorporates process-based understanding of tree growth, and predicts how climatic variables interact seasonally to limit photosynthesis and other processes; the other utilizes physiological thresholds, defined with 3-PG, to construct decision-tree models to predict the distribution of 15 different tree species. For each type of model, some measure of their reliability was independently assessed. Two of those assessments (LAI_{max} and disturbance) were
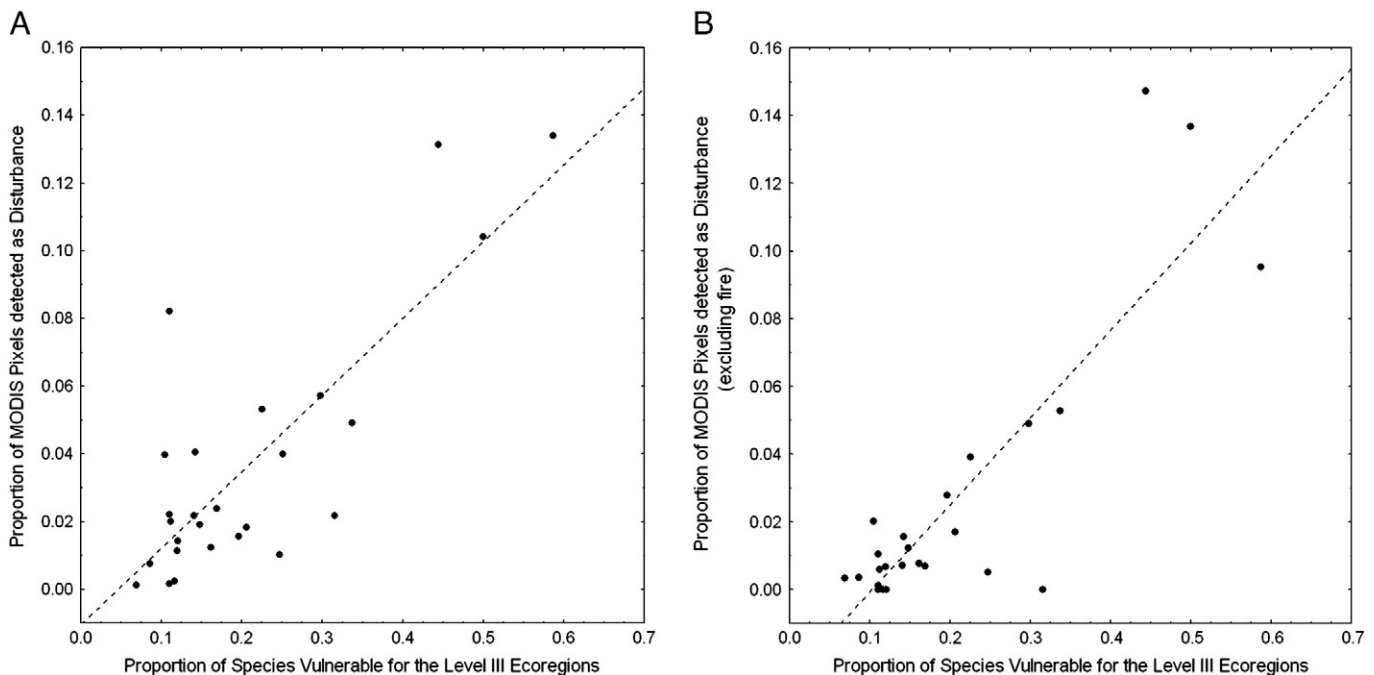
Fig. 5. (A) Relationship between the predicted proportion of vulnerable species within ecoregions fully contained in the study area (N = 25) and the proportion of cells recognized from MODIS imagery as disturbed for any cause ($r^2 = 0.65$, $p < 0.001$, SE = 0.080) and (B) with disturbances other than fire ($r^2 = 0.73$, $p < 0.001$, SE = 0.072).

based on remote sensing. It is possible that predictions of the beginning and end of the growing season might also be assessed more precisely in the future via remote sensing.

The ability to predict where disturbances are most likely to occur, and to offer an explanation is a valuable combination. In the future, if climatic conditions continue to change at accelerated rates, we would expect field surveys to report species in some places being replaced with those that have become more competitive, and less vulnerable to disturbance. A range of modeling approaches should be encouraged to meet the challenges ahead.

References

Allen, C. D., & Breshears, D. D. (1998). Drought-induced shift of a forest–woodland ecotone: Rapid landscape response to climate variation. *Proceedings of the National Academy of Sciences (USA)*, *95*, 14839–14842.

Allen, C. D., Macalady, A. K., Chenchouni, H., Bachelet, D., McDowell, N., et al. (2010). A global overview of drought and heat-induced tree mortality reveals emerging climate change risks of forests. *Forest Ecology & Management*, *259*, 660–684.

Beier, C. M., Sink, S. E., Hennon, P. E., D'Amore, D. V., & Juday, G. P. (2008). Twentieth-century warming and the dendroclimatology of declining yellow-cedar forests in southeastern Alaska. *Canadian Journal of Forest Research*, *38*, 1319–1334.

Bentz, B. J., Régnière, J., Fettig, C. J., Hansen, E. M., Hayes, J. L., et al. (2010). Climate change and bark beetles of the western United States and Canada: Direct and indirect effects. *BioScience*, *60*, 602–613.

Bristow, K. L., & Campbell, G. S. (1984). On the relationship between incoming solar radiation and daily maximum and minimum temperature. *Agricultural and Forest Meteorology*, *31*, 156–166.

Churkina, G., & Running, S. W. (1998). Contrasting climatic controls on the estimated productivity of global terrestrial biomes. *Ecosystems*, *1*, 206–215.

Cohen, W. C., & Goward, S. N. (2004). Landsat's role in ecological applications of remote sensing. *BioScience*, *54*, 535–546.

Coops, N. C., & Waring, R. H. (2001). Estimating maximum potential site productivity and site water stress of the eastern Siskiyous using 3-PGS. *Canadian Journal of Forest Research*, *31*, 143–154.

Coops, N. C., & Waring, R. H. (2011). Estimating the vulnerability of fifteen tree species under changing climate in the Northwest North America. *Ecological Modelling*, doi: 10.1016/j.ecolmodel.2011.03.033 (on line).

Coops, N. C., Waring, R. H., Beier, C., Roy-Jauvin, R., & Wang, T. (2011). Modeling the occurrence of fifteen coniferous species throughout the Pacific Northwest of North America using a hybrid approach of a generic process-based growth model and decision tree analysis. *Applied Vegetation Science*, doi:10.1111/j.1654-109X.2011.01125.x (on line).

Coops, N. C., Waring, R. H., & Landsberg, J. J. (1998). Assessing forest productivity in Australia and New Zealand using a physiologically-based model driven with averaged monthly weather data and satellite derived estimates of canopy photosynthetic capacity. *Forest Ecology and Management*, *104*, 113–127.

Coops, N. C., Waring, R. H., & Landsberg, J. J. (2001). Estimation of potential forest productivity across the Oregon transect using satellite data and monthly weather records. *International Journal of Remote Sensing*, *22*, 3797–3812.

Coops, N. C., Waring, R. H., & Moncrieff, J. B. (2000). Estimating mean monthly incident solar radiation on horizontal and inclined slopes from mean monthly temperature extremes. *International Journal of Biometeorology*, *44*, 204–211.

Coops, N. C., Waring, R. H., & Schroeder, T. A. (2009). Combining a generic process-based productivity model and a statistical classification method to predict the presence and absence of tree species in the Pacific Northwest, U.S.A.. *Ecological Modelling*, *220*, 1787–1796.

Coops, N. C., Waring, R. H., Wulder, M. A., & White, J. C. (2009). Prediction and assessment of bark beetle-induced mortality of lodgepole pine using estimates of stand vigor derived from remotely sensed data. *Remote Sensing of Environment*, *12*, 1058–1066.

Coppin, P. I., Jonckheere, K., Nackaerts, K., & Muys, B. (2004). Digital change detection methods in ecosystem monitoring: A review. *International Journal of Remote Sensing*, *10*, 1565–1596.

Crimmins, S. M., Dobrowski, S. Z., Greenberg, J. A., Abatzglous, J. T., & Mynsberge, A. R. (2011). Changes in climatic water balance drive downhill shifts in plant species' optimum elevations. *Science*, *331*, 324–327.

De'ath, G. (2002). Multivariate regression trees: A new technique for modeling species–environment relationships. *Ecology*, *83*, 1105–1117.

Foody, G. M., Palubinskas, G., Lucas, R. M., Curran, P. J., & Honzak, M. (1996). Identifying terrestrial carbon sinks: Classification of successional stages in regenerating tropical forest from Landsat TM data. *Remote Sensing of Environment*, *55*, 205–216.

Franklin, S. E. (2010). *Remote sensing for biodiversity and wildlife management.* New York: McGraw-Hill.

Franklin, J. F., & Dyrness, C. T. (1973). *Natural vegetation of Oregon and Washington.* United States Forest Service General Technical Report PNW-8. Portland, Oregon, USA.

Gedalof, Z., & Smith, D. J. (2001). Interdecadal climate variability and regime-scale shifts in Pacific North America. *Geophysical Research Letters*, *28*, 1515–1518.

Gong, P., & Xu, B. (2003). Remote sensing of forests over time: Change types, methods, and opportunities. In M. A. Wulder, & S. E. Franklin (Eds.), *Remote sensing of forest environments: concepts and case studies* (pp. 301–333). Massachusetts: Kluwer Academic Publishers.

Goward, S. N., Cruickshanks, G. D., & Hope, A. S. (1985). Observed relation between thermal emission and reflected spectral radiance of a complex vegetated landscape. *Remote Sensing of Environment*, *18*, 137–146.

Hadley, J. L. (2000). Effect of daily minimum temperature on photosynthesis in eastern hemlock *Tsuga canadensis* L. in autumn and winter. *Arctic, Antarctic, & Alpine Research*, *32*, 368–374.

Hember, R. A., Coops, N. C., Black, T. A., & Guy, R. D. (2010). Simulating gross primary production across a chronosequence of coastal Douglas-fir stands with a production efficiency model. *Agricultural & Forest Meteorology*, *150*, 238–253.

Huang, C., Goward, S. N., Masek, J. G., Thomas, N., Zhu, Z., & Vogelmann, J. E. (2010). An automated approach for reconstructing recent forest disturbance history using dense Landsat time series stacks. *Remote Sensing of Environment*, *114*, 183–198.

Hungerford, R. D., Nemani, R. R., Running, S. W., & Coughlan, J. C. (1989). MT-CLIM: A mountain microclimate simulation model. *USDA Forest Service Research Paper.* INT-414, Ogden, UT.

Huston, M. A., & Wolverton, S. (2009). The global distribution of net primary production: Resolving the paradox. *Ecological Monographs*, *79*, 343–377.

IPCC (2007). Summary for policymakers. In S. Solomon, D. Qin, M. Manning, M. Marquis, K. B. Averyt, M. Tignor, H. L. MillerJr., & Z. Chen (Eds.), *Climate change 2007: The physical science basis. Contribution of Working Group I to the Fourth Assessment Report of the Intergovernmental Panel on Climate Change*. Cambridge, UK: Cambridge University Press.

Iverson, L. R., & Prasad, A. M. (1998). Predicting abundance of 80 tree species following climate change in the eastern United States. *Ecological Monographs*, *68*, 465–485.

Jackson, S. T., Betancourt, J. L., Booth, R. K., & Gray, S. T. (2009). Ecology and the ratchet of events: Climate variability, niche dimensions, and species distributions. *Proceedings of the National Academy of Science (U.S.A.)*, *106*, 19685–19692.

Jolly, W., Dobbertin, M. M., Reichstein, M., & Zimmermann, N. (2005). Divergent vegetation growth responses to the 2003 heat wave in the Swiss Alps. *Geophysical Research Letters*, *109*, doi:10.1029/2004JD004959.

Justice, C. D., Giglio, L., Korontzi, S., Owens, J., Morisette, J. T., Roy, D., et al. (2002). The MODIS fire products. *Remote Sensing of Environment*, *83*, 244–262.

Kimball, J. S., McDonald, K. C., Running, S. W., & Frolking, S. E. (2004). Satellite radar remote sensing of seasonal growing season for boreal and subalpine evergreen forests. *Remote Sensing of Environment*, *90*, 243–258.

Kimball, J. S., Running, S. W., & Nemani, R. (1997). An improved method for estimating surface humidity from daily minimum temperature. *Agricultural and Forest Meteorology*, *85*, 87–98.

Landsberg, J. J., & Waring, R. H. (1997). A generalised model of forest productivity using simplified concepts of radiation-use efficiency, carbon balance and partitioning. *Forest Ecology and Management*, *95*, 209–228.

Landsberg, J. J., & Waring, R. H. (2004). Top-down models and flux measurements are complementary methods of estimating carbon sequestration by forests: Illustrations using the 3-PG model. In M. Mencuccini, J. Grace, J. Moncrieff, & K. G. McNaughton (Eds.), *Forest at the Land–Atmosphere Interface*. Cambridge, Mass: CABI Publishing.

Landsberg, J. J., Waring, R. H., & Coops, N. C. (2003). Performance of the forest productivity model 3-PG applied to a wide range of forest types. *Forest Ecology & Management*, *172*, 199–214.

Lathrop, R. G., Jr., Aber, J. D., & Bognar, J. A. (1995). Spatial variability of digital soil maps and its impact on regional ecosystem modeling. *Ecological Modelling*, *82*, 1–10.

Law, B. E., Turner, D., Campbell, J., Sun, O. J., Van Tuyl, S., et al. (2004). Disturbance and climate effects on carbon stocks and fluxes across western Oregon USA. *Global Change Biology*, *10*, 1429–1444.

Lefsky, M. A., Cohen, W. B., Parker, G. G., & Harding, D. J. (2002). Lidar remote sensing for ecosystem studies. *BioScience*, *52*, 19–30.

Mäkelä, A., Landsberg, J., Alan, R., Ek, A. R., Burk, T. E., et al. (2000). Process-based models for forest ecosystem management: current state of the art and challenges for practical implementation. *Tree Physiology*, *20*, 289–298.

Manter, D. K., Reeser, P. W., & Stone, J. K. (2005). A climate-based model for predicting geographic variation in Swiss needle cast severity in the Oregon Coast Range. *Phytopathology*, *86*, 1256–1265.

Mantua, N. J. (2001). The Pacific Decadal Oscillation. In M. C. McCracken, & J. S. Perry (Eds.), *The Encyclopedia of Global Environmental Change. The Earth System: physical and chemical dimension of global environmental change*, *1*. (pp. 592–594) Summerset, New Jersey, USA: John Wiley & Sons.

Mildrexler, D. J., Zhao, M. S., Heinsch, F. A., & Running, S. W. (2007). A new satellite-based methodology for continental-scale disturbance detection. *Ecological Applications*, *17*, 235–250.

Mildrexler, D. J., Zhao, M., & Running, S. W. (2009). Testing a MODIS Global Disturbance Index across North America. *Remote Sensing of Environment*, *113*, 2103–2117.

Mote, P. W., Parson, E. A., Hamlet, A. F., Ideker, K. N., Keeton, W. S., Lettenmaier, D. P., et al. (2003). Preparing for climate change: The water, salmon, and forests of the Pacific Northwest. *Climatic Change*, *61*, 45–88.

Mote, P. W., & Salathe, E. P. (2010). Future climate in the Pacific Northwest. *Climatic Change*, *102*, 29–50.

Nemani, R. R., Running, S. W., Pielke, R. A., & Chase, T. N. (1996). Global vegetation cover changes from course resolution satellite data. *Journal of Geophysical Research*, *101*, 7157–7162.

Nightingale, J. M., Coops, N. C., Waring, R. H., & Hargrove, W. W. (2007). Comparison of MODIS gross primary production estimates for forests across the USA with those generated by a simple process model, 3-PG. *Remote Sensing of Environment*, *109*, 500–509.

Nightingale, J. M., Phinn, S. R., & Held, A. A. (2004). Ecosystem process models at multiple scales for mapping tropical forest productivity. *Progress in Physical Geography*, *28*, 241.

Price, J. C., & Bausch, W. C. (1995). Leaf area index estimation from visible and near-infrared reflectance data. *Remote Sensing of Environment*, *52*, 55–75.

Raffa, K. F., Aukema, B. H., Bentz, B. J., Carroll, A. L., Hicke, J. A., et al. (2008). Cross-scale drivers of natural disturbances prone to anthropogenic amplification: The dynamics of bark beetle eruptions. *BioScience*, *58*, 501–517.

Rehfeldt, G. E., Crookston, N. L., Warwell, M. V., & Evans, J. S. (2006). Empirical analysis of plant–climate relationships for the western United States. *International Journal of Plant Science*, *167*, 1123–1150.

Rehfeldt, G. E., Ferguson, D. E., & Crookston, N. L. (2009). Aspen, climate, and sudden decline in western USA. *Forest Ecology & Management*, *258*, 2353–2364.

Rignot, E., Salas, W. A., & Skole, D. L. (1997). Mapping deforestation and secondary growth in Rondonia, Brazil, using imaging radar and thermatic mapper data. *Remote Sensing of Environment*, *59*, 167–179.

Running, S. W. (1980). Environmental and physiological control of water flux through *Pinus contorta*. *Canadian Journal of Forest Research*, *10*, 82–91.

Running, S. W., Waring, R. H., & Rydell, R. A. (1975). Physiological control of water flux in conifers: A computer simulation model. *Oecologia*, *18*, 1–16.

Runyon, J., Waring, R. H., Goward, S. N., & Welles, J. W. (1994). Environmental limits on net primary production and light-use efficiency across the Oregon transect. *Ecological Applications*, *4*, 226–237.

Spanner, M., Johnson, L., Miller, J., McCreight, R., Freemantle, J., et al. (1994). Remote sensing of seasonal leaf area indices across the Oregon Transect. *Ecological Applications*, *4*, 258–271.

Spittlehouse, D. L. (2008). Climate change, impacts, and adaptation scenarios: Climate change and forest and range management in British Columbia. : B.C. Ministry of Forests & Range, Research Branch, Victoria, British Columbia Technical Report 045.

Sutherst, R. W. (2003). Prediction of species geographical ranges. *Journal of Biogeography*, *30*, 805–816.

Swenson, J. J., Waring, R. H., Fan, W., & Coops, N. (2005). Predicting site index with a physiologically based growth model across Oregon, USA. *Canadian Journal of Forest Research*, *35*, 1697–1707.

Thorne, J. H., Morgan, B. J., & Kennedy, J. A. (2008). Vegetation change over sixty years in the Central Sierra Nevada, California, USA. *Madrono*, *55*, 223–237.

Thuiller, W., Albert, C., Araujo, M. B., Berry, P. M., Cabeza, M., et al. (2008). Predicting global change impacts on plant species' distributions: Future challenges. *Perspectives in Plant Ecology, Evolution and Systematics*, *9*, 137–152.

Treuhaft, R. N., Chapman, B. D., dos Santos, J. R., Goncalves, F. G., Dutra, L. V., et al. (2009). Vegetation profiles in tropical forests from multibaseline interferometric synthetic aperture radar, field, and lidar measurements. *Journal of Geophysical Research*, *114*, D23110, doi:10.1029/2008JD011674.

Trouet, V., & Taylor, A. H. (2009). Multi-century variability in the Pacific North American circulation pattern reconstructed from tree rings. *Climatic Dynamics*, doi:10.1007/s00382-009-0605-9.

Turner, D. P., Ritts, W. D., Cohen, W. B., Gower, S. T., Running, S. W., et al. (2006). Evaluation of MODIS NPP and GPP products across multiple biomes. *Remote Sensing of Environment*, *102*, 282–292.

Wang, T., Hamann, A., Spittlehouse, D. L., & Aitken, S. N. (2006). Development of scale-free climate data for western Canada for use in resource management. *International Journal of Climatology*, *26*, 383–397.

Waring, R. H. (1983). Estimating forest growth and efficiency in relation to canopy leaf area. *Advances in Ecological Research*, *13*, 326–354.

Waring, R. H. (2000). A process model analysis of environmental limitations on growth of Sitka spruce plantations in Great Britain. *Forestry*, *73*, 65–79.

Waring, R. H., & Franklin, J. F. (1979). Evergreen coniferous forests of the Pacific Northwest. *Science*, *204*, 1380–1386.

Waring, R. H., & Major, J. (1964). Some vegetation of the California coastal redwood region in relation to gradients of moisture, nutrients, light, and temperature. *Ecological Monographs*, *34*, 167–215.

Waring, R. H., & McDowell, N. (2002). Use of a physiological process model with forestry yield tables to set limits on annual carbon balances. *Tree Physiology*, *22*, 179–188.

Waring, R. H., Milner, K. S., Jolly, W. M., Phillips, L., & Mcwethy, D. (2005). A basis for predicting site index and maximum growth potential across the Pacific and Inland Northwest U.S.A. with a MODIS satellite-derived vegetation index. *Forest Ecology and Management*, *228*, 285–291.

Waring, R. H., & Running, S. W. (2007). *Forest ecosystems: Analysis at multiple scales.* San Diego, California: Academic Press.

Westerling, A. L., Hidalgo, H. G., Cayan, D. R., & Swetnam, T. W. (2006). Warming and earlier spring increase western U.S. forest wildfire activity. *Science*, *313*, 940–943.

White, M. A., de Beurs, K. M., Didan, K., Inouye, D. W., Richardson, A. D., et al. (2009). Intercomparison, interpretation, and assessment of spring phenology in North America estimated from remote sensing from 1982–2006. *Global Change Biology*, *15*, 2335–2359.

White, J. D., Running, S. W., Nemani, R., Keane, R. E., & Ryan, K. C. (1997). Measurement and remote sensing of LAI in Rocky Mountain ecosystems. *Canadian Journal of Forest Research*, *27*, 1714–1727.

Whitehead, D., Boelman, N. T., Turnbull, M. H., Griffin, K. L., Tissue, D. T., et al. (2005). Photosynthesis and reflectance indices for rainforest species in ecosystems undergoing progression and retrogression along a soil fertility chronosequence in New Zealand. *Oecologia*, *144*, 233–244.

Woods, A., Coates, K. D., & Hamann, A. (2005). Is an unprecedented *Dothistroma* needle blight epidemic related to climate change? *BioScience*, *55*, 761–769.

Zhao, M., & Running, S. W. (2010). Drought-induced reduction in global terrestrial net primary production from 2000 through 2009. *Science*, *329*, 940–943.

Zheng, D., Hunt, E. R., Jr., & Running, S. W. (1996). Comparison of available soil water capacity estimated from topography and soil series information. *Landscape Ecology*, *11*, 3–14.